Conductance and assembly of quasi-1D coordination chain molecular junctions with triazole derivatives

Zelin Miao,[a] Xiaoyun Pan,[b] and Maria Kamenetska[a,b,c*]

[a] *Division of Materials Science and Engineering, Boston University, Boston, Massachusetts, 02215, United States*

[b] *Department of Chemistry, Boston University, Boston, Massachusetts, 02215, United States*

[c] *Department of Physics, Boston University, Boston, Massachusetts, 02215, United States*

E-mail: mkamenet@bu.edu

ABSTRACT

Incorporating transition metal atoms into metal-molecule-metal junctions presents opportunities for exploring the electronic properties of coordination complexes, organometallics and metal-organic materials on the single molecule level. Recent single molecule conductance studies have shown that in situ incorporation of electrode metal atoms into coordination chains formed in the junction can occur with deprotonated, negatively charged organic ligands, such as imidazolate (Im^-) anion. However, the mechanism and chemical principles, such as the role of the charge state of the ligand, for the construction of such coordination chains are still debated. Here, we probe the role of the ligand charge state and electronic structure in single-molecule conductance and formation of metal-molecule coordination chains. We perform break junction measurements with triazole isomers, which can bridge junctions both in their neutral and charged forms, and find that prior deprotonation of the ligands is not required for coordination complex assembly, but can affect the molecular conductance and junction formation probability. Our results indicate that coordination chains can form with neutral ligands, as long as the electron density in the frontier MOs is concentrated at the binding sites and along the direction of pulling, promoting ligand binding and incorporation of gold atoms into the junction during elongation. Our findings may provide insight into design principles for in situ assembled molecular wires with transition metal atoms and open the door to electronic and spintronic studies of such materials.

MAIN

Incorporating transition metal atoms into molecular junctions has the potential to expand the scope of phenomena in nanoscale devices due to increased spin and orbital degrees of freedom.[1,2] Prior studies suggest that metal atom-containing junctions can serve as qubits,[3–5] switches,[6–9] spin valves,[10–12] and other memory and spintronic devices.[13–15] However, significant challenges to incorporating molecules with metal cores persist. We and others have recently shown that the donor-acceptor intramolecular interactions that characterize many inorganic coordination complexes are sometimes incompatible with the junction environment and lead to distortion and disassembly of the ex situ synthesized complexes on electrode surfaces.[16–19]

An alternative avenue towards assembly of the metal-atom containing junctions is *in situ* organometallic or coordination chain formation from organic precursors. We and others have demonstrated that extraction of gold atoms from the electrode and into the molecular wire can occur with certain ligands during junction elongation.[20–22] For example, our previous study of imidazole (Im), depicted in **Figure 1a**, shows that this heterocyclic compound with two non-adjacent nitrogen atoms (N1 and N3), once deprotonated to imidazolate (Im^-), can bridge source-drain nanogaps through dative interaction between nitrogen and undercoordinated gold surface sites to form molecular junctions.[22–25] Upon further tip retraction, longer chains composed of Im^--Au-Im^- are generated, as schematically illustrated in **Figure 1b**. Other molecular systems, including isocyano-terminated benzenes[20] and the unprotected terminal alkynes,[21,26] exhibit similar behavior, suggesting that this bottom-up strategy is a promising direction for achieving such functional metal-containing molecular devices.

In most prior work, the precursor ligands are organic anions, suggesting that charged species are required for assembly to occur. For example, our published results showed that the presence of the negative charge on the Im^- molecule could strengthen the Au-N bond and allow for the disruption of the gold electrode and the incorporation of gold atoms into the junction.[22] Yet the exact molecular mechanism of chain formation remains unclear.[27]

Here, we examine the chemical requirements for the in situ coordination chain assembly by studying the conductance and junction formation with imidazole variants—triazoles. The molecular structures of two triazole isomers, 1,2,4-triazole (Tr124) and 1,2,3-triazole (Tr123), are shown in **Figure 1c**. These isomers and their derivatives are commonly used organic ligands for applications requiring robust binding to transition metals through the electron lone pairs on the

nitrogens, such as for the synthesis of coordination compounds with significant spin-crossover properties,[28,29] or as corrosion inhibitors to passivate metal surfaces (e.g., copper and steel) in extreme conditions.[30,31] Here, we use them to bridge gold electrodes to form molecular junctions. Both triazole scaffolds contain three potential gold-binding sites—one pyrrole nitrogen (-NH-) and two tertiary amines (=N-, pyridine-like nitrogen atoms).[22,32,33] When dissolved in water, each isomer exists as a pair of tautomers accessed by intermolecular double-proton transfer with low activation barriers[34–36], as indicated by tautomeric equilibriums shown in the schemes (**Figure 1c**). The tautomeric isomerization of neutral molecules exposes two binding groups either at adjacent (4*H*-Tr124 and 1*H*-Tr123) or non-adjacent (1*H*-Tr124 and 2*H*-Tr123) positions. In basic conditions, when the pyrrole nitrogen is deprotonated to form triazolide anions ($Tr124^-$ and $Tr123^-$), an additional nitrogen anchor site to gold is exposed.

By measuring the conductance and 1D molecular chain assembly with triazoles in different solvent environments, we establish the transport characteristics of triazole-based molecular junctions in the neutral and anionic states. Specifically, our experimental results show that both triazole isomers in the neutral state can form single-molecule junctions and assemble into molecular chains, suggesting that ionic charge is not essential for chain formation. Furthermore, deprotonation facilitates electron transport and chain formation probability of Tr123 but lowers the conductance and broadens the signatures of Tr124. By comparing these experimental observations with DFT calculations, we are able to infer which molecular orbital features contribute to successful chain formation. We find that the structure of the frontier molecular orbitals (MOs) and the availability of the lone pairs on non-adjacent nitrogens for binding are the decisive factors in the probability of in situ chain assembly. Our work here may help uncover and establish the chemical requirements for incorporating transition metal atoms into quasi-1D molecular wires in the junctions.

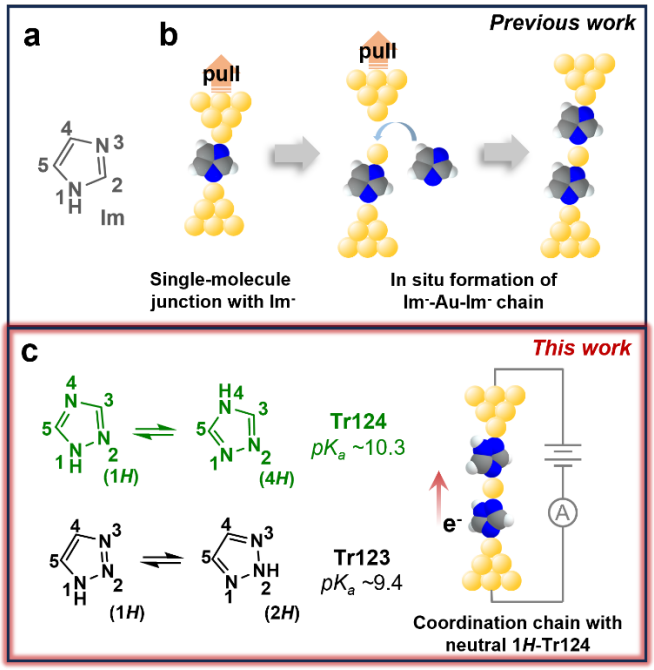

Figure 1. **(a)** Chemical structure of imidazole (Im) investigated in previous work.[22] **(b)** Schematic illustration of a single Im^- molecule bound between gold electrodes and the in situ metal-molecule chain formation with Im^- upon junction elongation. **(c)** Chemical structures and tautomeric isomerization of 1,2,4-triazole (Tr124) and 1,2,3-triazole (Tr123) in aqueous solutions. The pK_a values of Tr124 and Tr123 are ~10.3 and ~ 9.4, respectively.[37] We show in this work that coordination chains can also be constructed with neutral Tr123 and Tr124. Color code: N, blue; C, gray; H, white; Au, yellow.

We perform single-molecule conductance measurements using a home-built scanning tunneling microscope break-junction (STM-BJ) instrument following established protocols, as previously described (see **SI** for more details).[38,39] In a typical experiment, we repeatedly smash in and pull apart two gold electrodes with sub-angstrom precision to form source-drain nanogaps under a constant bias. These gaps can be bridged by molecules that self-assemble between the gold electrodes through electron donor sites on the molecule. Conductance (current/voltage) is measured as a function of the relative displacement of electrodes during junction elongation at a bias of 100 mV or 500 mV. Thousands of such measurements are recorded and compiled into conductance histograms which are fit to Gaussian curves to extract the most probable conductance values. We measure the two triazole isomers from **Figure 1c** and their methylated derivatives discussed further below in organic solvents, *N,N*-dimethylformamide (DMF) and 1,2,4-tricholorobenzene (TCB), or dip-coated onto the substrates out of aqueous solutions as described in the **SI** and in our previous work.[22,40,41] Measurements in aqueous liquid conditions using the

wax-coated tip are also performed and shown in the **SI** for comparison to the dip-coated measurements. Both dried and aqueous conditions yield the same molecular conductance values, but the signal-to-noise is higher in dried dip-coated samples (**Figure S1**).[22] Therefore, all measurements shown in the manuscript are performed in dry conditions except those in organic solvents.

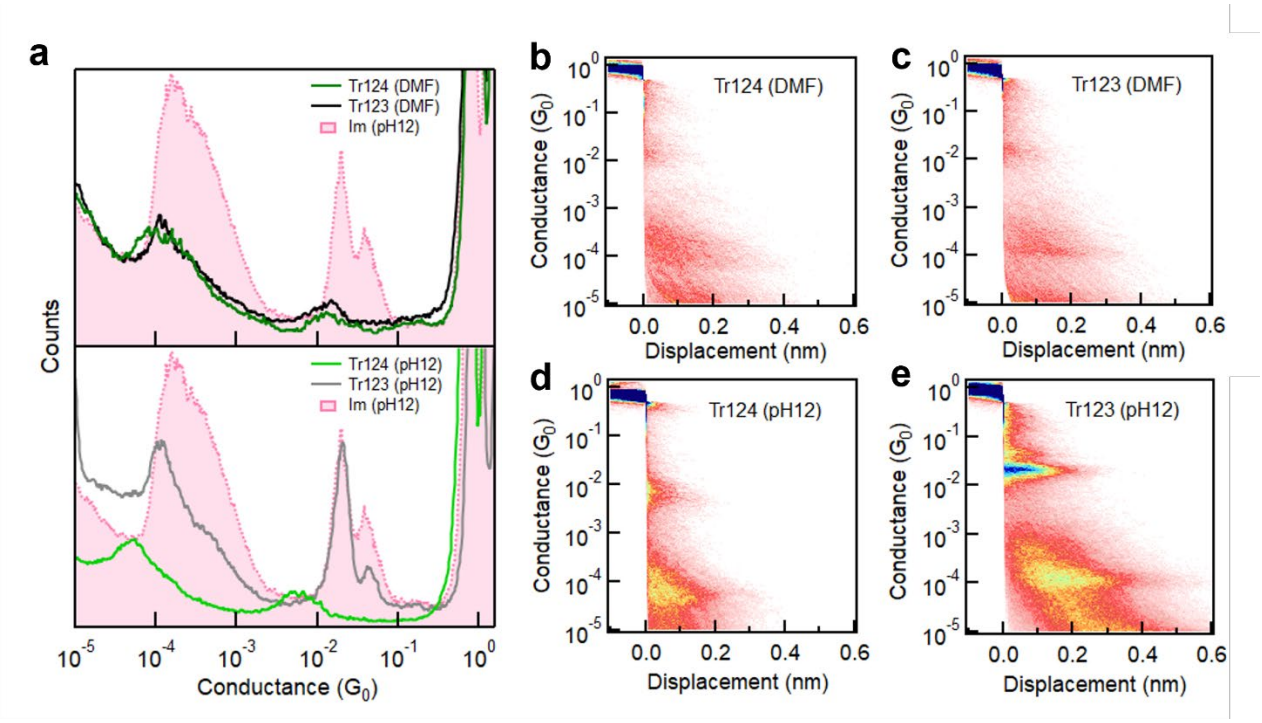

Figure 2. **(a)** Top: overlaid 1D log-binned conductance histograms of Tr124 (green) and Tr123 (black) measured in DMF solutions using the wax-coated tips to provide ionic isolation. Bottom: conductance histograms of $Tr124^-$ and $Tr123^-$ dip-coated on gold samples from pH 12 aqueous solutions. Conductance histogram of Im^- is plotted for comparison.[22] All histograms are constructed from at least 4000 consecutive individual traces without any data selection. **(b-c)** 2D conductance-displacement histograms compiled from thousands of traces of Tr123 and Tr124 in DMF solutions or **(d-e)** of $Tr123^-$ and Tr 124^- dip-coated from water at pH 12.

We first measure the conductance of Tr124 and Tr123 in DMF solutions, where the neutral motifs of triazoles are predominant, using wax-coated tips to suppress the ionic background current.[42] The histograms for both molecules, shown in **Figure 2a** (top panel), are compiled from 4000 consecutive measured traces without any data selection. We observe similar conductance features for both isomers within two distinct regimes at ~10^{-2} G_0 (high-G) and ~10^{-4} G_0 (low-G). Compared to our previous work on Im^- replotted here in pink, this suggests that the high-G peaks result from one or several molecules bound in parallel, similar to Im^- (**Figure 1b**, left), while the

low-G features are due to chain formation where the molecules are bound in series (**Figure 1b** and **1c**, right).[22, 41] Notably, the extension lengths that junctions can sustain for both isomers in low-G are ~ 4 Å, approximately double that of high-G plateaus, as shown in 2D conductance-displacement histograms (**Figure 2b** and **2c**). The presence of both the high- and low-G features in triazole data, their similarity to Im^- signatures, and the relative extensions indicate that neutral triazoles in DMF can bind to gold through opposite tertiary amines present in both isomers (N2/N4 in 1*H*-Tr124 and N1/N3 in 2*H*-Tr123 as shown in **Figure 1c**), analogously to the geometry of Im^- junctions.[22,25]

The most probable high-G conductance values for Tr124 and Tr123 are 1.27×10^{-2} G_0 and 1.31×10^{-2} G_0, respectively, which are ~35 % lower than the conductance of Im^-. We note that the amplitude of the conductance peaks with neutral triazoles is also lower than with Im^- measured in dried condition, for both high-G and low-G signatures. This feature may be due to the different environments in which the measurements were performed which we explore below. Nevertheless, these results collectively suggest that neutral triazole motifs, whether Tr124 or Tr123, can form extended metal-molecule chains in DMF and that anionic character is not required for in situ coordination complex assembly.

To test if the deprotonation of triazoles can affect their junction binding and transport characteristics, we perform break-junction measurements of Tr123 and Tr124 by depositing molecules from aqueous pH 12 solutions on gold. In such basic environments, where pH ≥ pK_a (**Figure 1c**), the equilibrium of both triazole molecules shifts towards the anionic states. The resulting conductance histograms compiled out of 5000 individual traces are plotted in the bottom panel of **Figure 2a**. In these conditions, the conductance characteristics of the two triazole anions are distinct. In both cases, we still observe high-G and low-G conductance signatures. Consulting 2D histograms of both isomers in **Figure 2d-e** we note that the low-G plateaus persist on average twice as long as high-G features, similar to their neutral analogs. However, with $Tr123^-$, the high-G value corresponding to the single molecule junction (highest amplitude peak) is found to be 2.01×10^{-2} G_0, which is in good agreement with the conductance of Im^-. This correspondence reveals that once it becomes deprotonated, $Tr123^-$ is likely to adopt a similar binding configuration as Im^- anchoring to gold through non-adjacent nitrogen atoms at N1 and N3 positions, while the N2 nitrogen in between has negligible impact on conductance or binding. Chain formation probability is also robust, as indicated by the high peak amplitude. In contrast, for anionic $Tr124^-$,

a broad peak with conductance of 5.39×10^{-3} G_0 (measured at 100 mV) occurs in the high-G region, which is significantly lower than the single molecule conductance of $Tr123^-$ and Im^-. The conductance of the chain is similarly lower than in $Tr123^-$ or in Im^-. We also note that $Tr124^-$ displays a lower chain formation yield as indicated by the decreased amplitude of its low-G feature compared to $Tr123^-$.

We supplement the conductance measurement of Tr124 in pH 12 shown above with measurements in pH 1.5, 3, and 9 in **Figure 3a** (see **Figure S2** for measurements of Tr123 at varying pH conditions). These pH conditions are selected to probe the distinct charged states of Tr124, which is characterized by two pK_a values;[37] at pH<2.2, the molecule is a triazolium cation $Tr124^+$; at pH>10.3, it becomes deprotonated to triazolide anion $Tr124^-$. We observe distinct signatures in each pH regime. At pH 1.5, there is a single broad peak at ~10^{-3} G_0. This feature has been previously attributed to through-space transport associated with the π-π stacks of two molecules bound on opposite electrodes.[22,43] These measurements are consistent with $Tr124^+$, which only has one unprotonated binding site. At pH 3, through-space transport is still present. However, the high-G and low-G bridging features start appearing at ~10^{-2} and 10^{-4} G_0 due to an equilibrium between triazolium cation and neutral triazole in this condition. At pH 9, π-π stacking features are gone, and the conductance resembles signatures of the neutral Tr124 molecule that we measured in DMF in **Figure 2a** (replotted in **Figure 3b**). We list the average single-molecule conductance (high-G) data in **Table 1** and note that the high-G conductance values of Tr124 in DMF and at pH=9 are within experimental error (see **SI** for more details). Notably, the conductance and amplitude of the broad high-G feature appearing at pH 12 (with applied bias of 500 mV) are distinct and lower than at pH 9. Based on these results, we conclude that the junction formation probability for the anionic $Tr124^-$ is lower than for neutral analog deposited from the aqueous environments. Control measurements of triazole isomers at each pH condition at different biases show no significant bias dependence for both high-G and low-G signatures (**Figure S3** and **S4**).

Table1. The most probable conductance values of high-G peaks (~ 10^{-2} G_0) of triazole derivatives with different solvents and pH conditions

	Solvent	pH	Conductance (experimental, G_0)
Im	H_2O	12	1.96×10^{-2}
Tr124	H_2O	12	7.03×10^{-3}
	H_2O	9	1.29×10^{-2}

	DMF	N/A	1.27×10^{-2}
1Me-Tr124	TCB	N/A	1.05×10^{-2}
Tr123	H_2O	12	2.01×10^{-2}
	H_2O	8	1.94×10^{-2}
	DMF	N/A	1.31×10^{-2}

To rule out the possibility of junction bridging of Tr124 through two adjacent nitrogen atoms, we measure the conductance of two Tr124 derivatives: 4-methyl-*4H*-1,2,4-triazole (4Me-Tr124) and 1-methyl-1,2,4-triazole (1Me-Tr124) in TCB (**Figure 3b**, see 2D conductance histogram in **Figure S5**). In these molecules, non-exchangeable methyl groups substitute the hydrogen atom[44] to block one of the nitrogen sites from binding with gold. We observe only a broad π-π stacking conductance signature at ~10^{-3} G_0 for 4Me-Tr124 in which only adjacent nitrogen binding sites are present, confirming that bridging the junction through adjacent nitrogen sites is unlikely. For 1Me-Tr124, the peak at ~10^{-2} G_0 is broadly consistent with neutral Tr124 measured in DMF and pH 9 aqueous solutions, with a slight shift to the lower value due to the methyl substituent.[45] These results further confirm that neutral Tr124 is responsible for the high-G single-molecule feature, as summarized in **Table 1**. Notably, the low-G conductance peak is also present with 1Me-Tr124 in this non-aqueous organic solvent, confirming that chain formation with neutral Tr124 analogs can occur. To summarize, our data suggest that we capture distinct charge states of Tr124 at different pH environments, and, more importantly, that the binding to gold electrodes through two tertiary amine nitrogens in neutral Tr124 can lead to more robust and higher conducting single-molecule junctions and low-G chains in comparison to its anionic analog (see the **SI** for the discussion regarding Tr123).

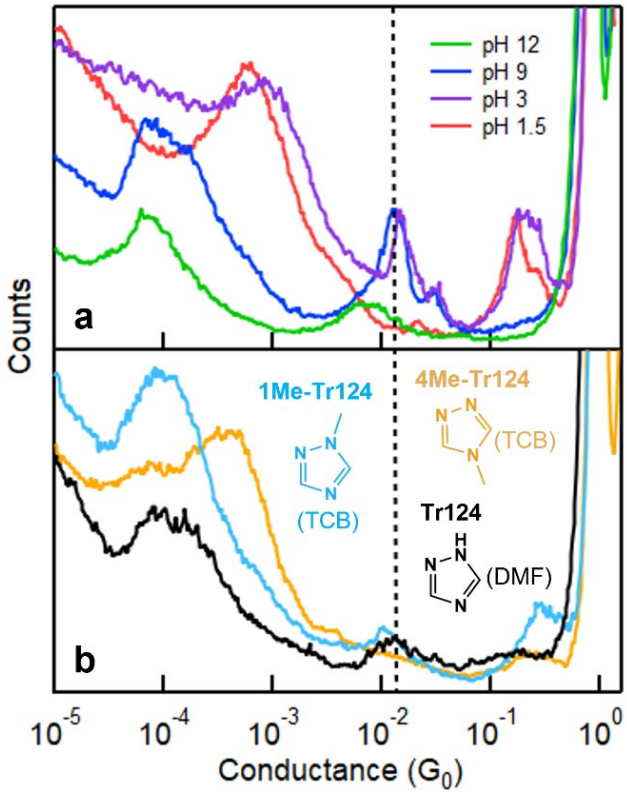

Figure 3. (a) Conductance measurements of Tr124 through molecular deposition out of aqueous solutions with varying pH values under bias of 500 mV. Dissolving molecules in neutral H_2O results in solution with pH~9. Each histogram is constructed from 5000 individual traces. **(b)** Conductance histograms of control molecules including 1-methyl-1,2,4-triazole (1Me-Tr124) and 4-methyl-*4H*-1,2,4-triazole (4Me-Tr124) measured in TCB solutions. Histogram for Tr124 measured in DMF from **Figure 2a** is reproduced here for convenience.

We turn to first-principles density functional theory (DFT) calculations to provide insights into the origin of different conductance trends and coordination chain formation with neutral and anionic Tr124 and Tr123 discussed above. FHI-aims package equipped with the AITRANSS module[46–48] and Perdew-Burke-Ernzerhof (PBE) density functional[49] is applied to calculate junction geometries, gas-phase molecular orbitals (MOs), and electron transport through the molecular junctions using previously established protocols[50] with details provided in the **SI**. The relaxed junction structures and transmission spectra for neutral and anionic systems are shown in **Figures 4a** and **4b**, respectively. In all cases, the most stable junction structures are formed with molecules bound through non-adjacent nitrogen atoms in agreement with experimental measurements. The binding energy of neutral N-Au bonds is characteristic of pyridine-gold type interactions at 0.4-0.5 eV, but the binding of the anionic species is ~ 1.5-2 eV (see **SI** for more

details of binding energy calculations).[25, 56] These results are consistent with our prior findings for the Im^- junction system.

The predicted transmission spectra of neutral Tr123 and Tr124 are shown in **Figure 4a**. We observe that the LUMO resonances are closer to E_F for these neutral motifs, suggesting that LUMO dominates transport at low bias for both molecules. The transmission at Fermi, indicated by a dashed line, is nearly identical for both molecules, consistent with the measured conductance of Tr123 and Tr124 in DMF solutions shown in **Figure 2a**.

In contrast, we find that the transport of anionic Tr124 and Tr123 junctions are HOMO-dominated because the transmission peaks at ~ -1.7 eV are closer to and have more overlap with E_F than the LUMO peaks at ~ 3.5 eV (**Figure 4b**). Calculated transmission values of $Tr123^-$ and $Tr124^-$ are 5.47×10^{-2} G_0 and 4.45×10^{-2} G_0, respectively. The difference is in qualitative agreement with our experimental observations that $Tr123^-$ has higher conductance than $Tr124^-$ (**Figure 2a)**. We note the general overestimation of DFT-based transport calculation compared to the measured conductance for single-molecule junctions is consistent with the disparity reported in previous studies.[51–55] We conclude that the differences in the energy alignment and reduced coupling of HOMO with E_F in the anionic triazoles are partially responsible for the lower conductance of the $Tr124^-$ compared to $Tr123^-$.

Frontier MOs of neutral and anionic Tr124 and Tr123 isomers relevant for junction binding and transport are depicted in **Figures 4c**, **d** and **e**, **f**, respectively. We observe σ character on both non-adjacent nitrogen atoms in HOMO or HOMO-1 (for 2*H*-Tr123) in all four species. The complete set of gas-phase MOs of all the triazole isomers are shown in **Figures S6** and **S7**. This result is consistent with prior studies showing that pyridine nitrogen binds to gold through the electron lone pairs in the σ framework, which is part of the filled states even if the main transmission channel is dominated by the molecular LUMO.[25,56] Specifically, in the neutral analogs, the high electron density at the non-adjacent nitrogens is concentrated in the σ-dominated and closely spaced HOMO and HOMO-1, indicating the availability of electron lone-pairs on those sites to bind to gold. The role of HOMO σ orbitals in junction binding is also evident in the eigenchannel analysis of neutral Tr123 and Tr124 shown in **Figures S8** and **S9**, respectively. We observe high electron density at the N-Au bonds in the filled part of the spectrum and note that it is aligned with the junction elongation direction. The π-LUMO orbitals which dominate transport are similar in their distribution across the two neutral molecules. Overall, this analysis is consistent

with experimentally determined similarity in junction yield and conductance values of neutral triazoles.

Turning to the anionic species, we note that the high electron density at the lone pair sites is also present in $Tr123^-$ on the closely spaced σ HOMO and HOMO-2. Similar to neutral triazoles, the resulting N-Au bond exhibits high electron density and aligns with the pulling direction, as illustrated in **Figure S10**. In contrast, in $Tr124^-$ gas-phase HOMO-2 is further below the HOMO, indicating a reduced ability of this MO to transfer charge to the gold during binding. The remaining HOMO orbital has a node, or no charge density, on the N4, as shown in **Figure 4e**, and is instead concentrated on the adjacent N1 and N2 nitrogen atoms. This change is reflected in the junction eigenchannel analysis for $Tr124^-$ in **Figure S11**, where less electron density is observed in the N-Au bond on $Tr124^-$, particularly in the HOMO resonance. The concentration of charge on the adjacent nitrogen atoms increases the likelihood of $Tr124^-$ binding to one electrode with both N1 and N2, as shown in **Figure S12**.[32] This geometry has a reduced binding energy between N4 and gold and may explain the shorter plateaus and the lower likelihood of chain assembly observed with $Tr124^-$. In **Figure S13**, we show that the transmission through such junctions where all three nitrogen atoms are bound to electrodes (which is only likely with $Tr124^-$) is quite distinct from the two-nitrogen bridging geometry and will broaden the conductance distribution observed with this molecule. Overall, the low density of the σ-MOs on the N4 and the large number of available geometries associated with $Tr124^-$ likely account for the broadness and low amplitude of its high-G conductance peak compared to its neutral analogues and to $Tr123^-$.

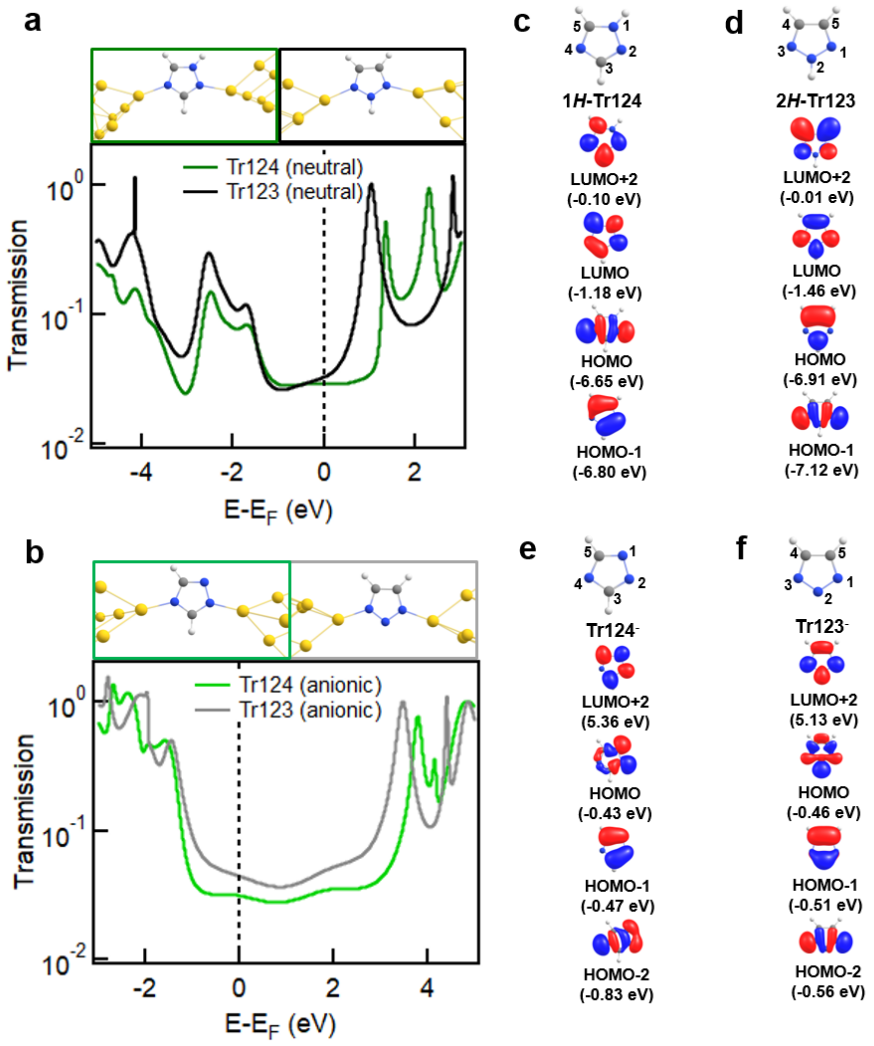

Figure 4. (a, b) Relaxed junction geometries with neutral and anionic Tr124 and Tr123 bound between two Au18 pyramids with the apex Au-Au distance corresponding to potential energy minimum (top) and the calculated transmission spectra (bottom). Frontier MOs of Tr124 and Tr123 in neutral **(c, d)** and anionic **(e, f)** forms and calculated using FHI-aims package with a "tight" basis set and the PBE functional (see **Figure S6** and **S7** for the complete pictures of MO plotting).

DFT transport calculations of the extended chains formed with anionic Tr123 and Tr124 are also shown in **Figure 5** (the spectra of the corresponding neutral analogs are displayed in **Figure S14**). We note that in terms of the chain configurations as well, Tr124$^-$ has numerous binding orientations with respect to the direction of the adjacent nitrogen atoms (dashed arrows in **Figure 5**, top), while Tr123$^-$ only has one symmetric geometry. Transport calculations in **Figure 5** (bottom) show that transmission through the distinct junctions of Tr124$^-$ chains varies at the

Fermi energy, which is in qualitatively agreement with the broadened conductance distribution we observe in experiments. Chain configurations where both N1 and N2 bind to one electrode as in **Figure S13** or to both electrodes (not shown) are also possible and may further broaden the conductance distribution measured with the $Tr124^-$ chains. The predicted conductance of the $Tr123^-$ chain is 1.96×10^{-4} G_0, which is higher than the predicted average of the $Tr124^-$ chains at 7.95×10^{-5} G_0, consistent with our experimental results. Overall, we conclude that the asymmetry of $Tr124^-$ and the associated asymmetric MOs with reduced density on the N4 result in numerous binding orientations of this molecule in the junction, which interferes in the formation of a well-defined single molecule coordination wire and contributes to a broad conductance distribution observed in experiment.

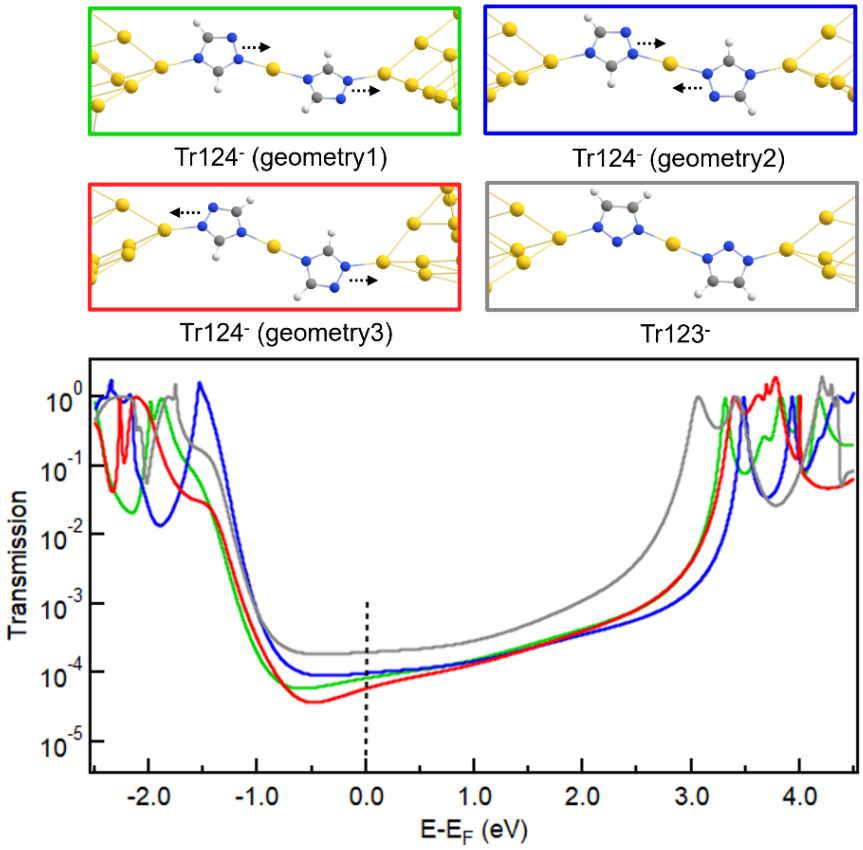

Figure 5. Junction structures with coordination chains comprising anionic $Tr123^-$ and accessible geometries of $Tr124^-$ with distinct arrangements of the two adjacent tertiary amines (=N-) with respect to the electrodes (indicated by the dashed arrows, top) and the corresponding transmission spectra (bottom). Configurations with one or both $Tr124^-$ molecule bound to dull gold electrodes through two adjacent nitrogens are also possible but are not included here. The number of electrons in the structure was adjusted to make the overall junction closed shell.

In conclusion, we evaluate the effect of the molecular charge states of triazole isomers on the transport properties of single molecule-metal junctions and on the chain structure formation. We demonstrate identical conductance signatures of Tr123 and Tr124 in their neutral motifs and the evidence of quasi-1D chain formation in both molecules even in the absence of overall linker charge. In contrast, upon deprotonation, anionic $Tr124^-$ displays significant conductance suppression and a broadened conductance signature in comparison to $Tr123^-$. DFT calculations corroborate our experimental observations and suggest that deficient electron density on non-adjacent pyridine-like nitrogen atoms of $Tr124^-$ in gas-phase MOs results in a less favorable bridging of the junction electrodes, hampering the quasi-1D chain formation. Instead, $Tr124^-$ is more likely to bind to a single electrode with two adjacent tertiary amine nitrogens, resulting in various geometries all with distinct conductance values which broaden and wash out the molecular signature. Numerous configurations of $Tr124^-$ are also possible in the chain configuration, where the conductance is similarly broadened. Overall, our work reveals that anionic character is not required for in situ assembly of coordination chains but that controlling the electron density distribution within the molecule is key to engineering effective linkers for chain formation. Our work also emphasizes the particular importance of the σ network for coordination complex assembly in the junction. It suggests that good alignment between the binding MOs and the direction of junction elongation is a prerequisite for incorporating gold atoms from the electrode into the junction. Taken together, this work provides insight into chemical strategies for modulating single-molecule conductance and coordination chain assembly via electronic structure tuning.

ASSOCIATED CONTENT

Supporting Information (SI)

STM-BJ procedure, sample-preparation, error analysis and computational details, conductance measurements of Tr123 with varying pH, bias-dependent controls, MOs of triazole isomers, eigenchannel analysis, binding energy and additional transmission spectra of junctions.

AUTHOR INFORMATION

Corresponding Author

Maria Kamenetska – E-mail: mkamenet@bu.edu

Notes

The authors declare no competing financial interest.

ACKNOWLEDGEMENTS

This work was supported by the National Science Foundation under award #2145276. Z.M. acknowledges support from a BUnano Cross-Disciplinary Fellowship. All authors appreciate support from the BU Photonics Center where the work was performed. The authors gratefully thank Dr. Brent Lawson and Sigifredo Luna for the useful discussions on DFT calculations.

REFERENCE

(1) Bogani, L., Wernsdorfer, W. Molecular Spintronics Using Single-Molecule Magnets. *Nat. Mater.* **2008**, *7*, 179–186.

(2) Vincent, R.; Klyatskaya, S.; Ruben, M.; Wernsdorfer, W.; Balestro, F. Electronic Read-out of a Single Nuclear Spin Using a Molecular Spin Transistor. *Nature* **2012**, *488*, 357–360.

(3) Gaita-Ariño, A.; Luis, F.; Hill, S.; Coronado, E. Molecular Spins for Quantum Computation. *Nat. Chem.* **2019**, *11*, 301–309.

(4) Thiele, S.; Balestro, F.; Ballou, R.; Klyatskaya, S.; Ruben, M.; Wernsdorfer, W. Electrically Driven Nuclear Spin Resonance in Single-Molecule Magnets. *Science* **2014**, *344*, 1135–1138.

(5) Fursina, A. A.; Sinitskii, A. Toward Molecular Spin Qubit Devices: Integration of Magnetic Molecules into Solid-State Devices. *ACS Appl. Electron. Mater.* **2023**, *5*, 3531–3545.

(6) Aragonès, A. C.; Aravena, D.; Cerdá, J. I.; Acís-Castillo, Z.; Li, H.; Real, J. A.; Sanz, F.; Hihath, J.; Ruiz, E.; Díez-Pérez, I. Large Conductance Switching in a Single-Molecule Device through Room Temperature Spin-Dependent Transport. *Nano Lett.* **2016**, *16*, 218–226.

(7) Wagner, S.; Kisslinger, F.; Ballmann, S.; Schramm, F.; Chandrasekar, R.; Bodenstein, T.; Fuhr, O.; Secker, D.; Fink, K.; Ruben, M.; Weber, H. B. Switching of a Coupled Spin Pair in a Single-Molecule Junction. *Nat. Nanotechnol.* **2013**, *8*, 575–579.

(8) Ormaza, M.; Abufager, P.; Verlhac, B.; Bachellier, N.; Bocquet, M. L.; Lorente, N.; Limot, L. Controlled Spin Switching in a Metallocene Molecular Junction. *Nat. Commun.* **2017**, *8*, No. 1974.

(9) Schwarz, F.; Kastlunger, G.; Lissel, F.; Egler-Lucas, C.; Semenov, S. N.; Venkatesan, K.; Berke, H.; Stadler, R.; Lörtscher, E. Field-Induced Conductance Switching by Charge-State Alternation in Organometallic Single-Molecule Junctions. *Nat. Nanotechnol.* **2016**, *11*, 170–176.

(10) Pal, A. N.; Li, D.; Sarkar, S.; Chakrabarti, S.; Vilan, A.; Kronik, L.; Smogunov, A.; Tal, O. Nonmagnetic Single-Molecule Spin-Filter Based on Quantum Interference. *Nat. Commun.* **2019**, *10*, No. 5565.

(11) Urdampilleta, M.; Klyatskaya, S.; Cleuziou, J.-P.; Ruben, M.; Wernsdorfer, W. Supramolecular Spin Valves. *Nat. Mater.* **2011**, *10*, 502–506.

(12) Singh, A. K.; Chakrabarti, S.; Vilan, A.; Smogunov, A.; Tal, O. Electrically Controlled Bimetallic Junctions for Atomic-Scale Electronics. *Nano Lett.* **2023**, *23*, 7775–7781.

(13) Timm, C.; Elste, F. Spin Amplification, Reading, and Writing in Transport through Anisotropic Magnetic Molecules. *Phys. Rev. B* **2006**, *73*, No. 235304.

(14) Schmaus, S.; Bagrets, A.; Nahas, Y.; Yamada, T. K.; Bork, A.; Bowen, M.; Beaurepaire, E.; Evers, F.; Wulfhekel, W. Giant Magnetoresistance through a Single Molecule. *Nat. Nanotechnol.* **2011**, *6*, 185–189.

(15) Bayliss, S. L.; Laorenza, D. W.; Mintun, P. J.; Kovos, B. D.; Freedman, D. E.; Awschalom, D. D. Optically Addressable Molecular Spins for Quantum Information Processing. *Science* **2020**, *370*, 1309–1312.

(16) Skipper, H. E.; May, C. V.; Rheingold, A. L.; Doerrer, L. H.; Kamenetska, M. Hard-Soft Chemistry Design Principles for Predictive Assembly of Single Molecule-Metal Junctions. *J. Am. Chem. Soc.* **2021**, *143*, 16439–16447.

(17) Knaak, T.; González, C.; Dappe, Y. J.; Harzmann, G. D.; Brandl, T.; Mayor, M.; Berndt, R.; Gruber, M. Fragmentation and Distortion of Terpyridine-Based Spin-Crossover Complexes on Au(111). *J. Phys. Chem. C* **2019**, *123*, 4178–4185.

(18) Rohlf, S.; Grunwald, J.; Jasper-Toennies, T.; Johannsen, S.; Diekmann, F.; Studniarek, M.; Berndt, R.; Tuczek, F.; Rossnagel, K.; Gruber, M. Influence of Substrate Electronic

Properties on the Integrity and Functionality of an Adsorbed Fe(II) Spin-Crossover Compound. *J. Phys. Chem. C* **2019**, *123*, 17774–17780.

(19) Ossinger, S.; Naggert, H.; Kipgen, L.; Jasper-Toennies, T.; Rai, A.; Rudnik, J.; Nickel, F.; Arruda, L. M.; Bernien, M.; Kuch, W.; Berndt, R.; Tuczek, F. Vacuum-Evaporable Spin-Crossover Complexes in Direct Contact with a Solid Surface: Bismuth versus Gold. *J. Phys. Chem. C* **2017**, *121* (2), 1210–1219.

(20) Vladyka, A.; Perrin, M. L.; Overbeck, J.; Ferradás, R. R.; García-Suárez, V.; Gantenbein, M.; Brunner, J.; Mayor, M.; Ferrer, J.; Calame, M. In-Situ Formation of One-Dimensional Coordination Polymers in Molecular Junctions. *Nat. Commun.* **2019**, *10*, No. 262.

(21) Song, K.; Lin, J.; Song, X.; Zhang, M.; Gu, Q.; Zang, Y.; Zhu, D. In Situ Creation of Organometallic Molecular Junctions via Terminal Alkynes. *J. Phys. Chem. C* **2023**, *127*, 8850–8855.

(22) Pan, X.; Lawson, B.; Rustad, A. M.; Kamenetska, M. PH-Activated Single Molecule Conductance and Binding Mechanism of Imidazole on Gold. *Nano Lett.* **2020**, *20*, 4687–4692.

(23) Mishchenko, A.; Zotti, L. A.; Vonlanthen, D.; Bürkle, M.; Pauly, F.; Cuevas, J. C.; Mayor, M.; Wandlowski, T. Single-Molecule Junctions Based on Nitrile-Terminated Biphenyls: A Promising New Anchoring Group. *J. Am. Chem. Soc.* **2011**, *133*, 184–187.

(24) Hybertsen, M. S.; Venkataraman, L.; Klare, J. E.; Whalley, A. C.; Steigerwald, M. L.; Nuckolls, C. Amine-Linked Single-Molecule Circuits: Systematic Trends across Molecular Families. *J. Phys.: Condens. Matter* **2008**, *20*, No. 374115.

(25) Kamenetska, M.; Quek, S. Y.; Whalley, A. C.; Steigerwald, M. L.; Choi, H. J.; Louie, S. G.; Nuckolls, C.; Hybertsen, M. S.; Neaton, J. B.; Venkataraman, L. Conductance and Geometry of Pyridine-Linked Single-Molecule Junctions. *J. Am. Chem. Soc.* **2010**, *132*, 6817–6821.

(26) Li, S.; Yu, H.; Chen, X.; Gewirth, A. A.; Moore, J. S.; Schroeder, C. M. Covalent Ag-C Bonding Contacts from Unprotected Terminal Acetylenes for Molecular Junctions. *Nano Lett.* **2020**, *20*, 5490–5495.

(27) Li, S.; Jiang, Y.; Wang, Y.; Hou, S. The Formation and Conducting Mechanism of Imidazole-Gold Molecular Junctions. *ChemistrySelect* **2021**, *6*, 2959–2965.

(28) Liu, M.; Han, X.; Huang, H.; Long, X.; Tan, B. Controllable Sensitivity Mechanism in an Energetic Compound of [FeII(Rtrz)$_6$] as a Molecular Switch. *Chem. Phys. Lett.* **2022**, *801*, No. 139682.

(29) Roubeau, O. Triazole-Based One-Dimensional Spin-Crossover Coordination Polymers. *Chem. Eur. J.* **2012**, *18*, 15230–15244.

(30) Wazzan, N.; Obot, I. B.; Fagieh, T. M. The Role of Some Triazoles on the Corrosion Inhibition of C1020 Steel and Copper in a Desalination Descaling Solution. *Desalination* **2022**, *527*, No. 115551.

(31) Li, W.; Tan, B.; Zhang, S.; Guo, L.; Ji, J.; Yan, M.; Wang, R. Insights into Triazole Derivatives as Potential Corrosion Inhibitors in CMP Process: Experimental Evaluation and Theoretical Analysis. *Appl. Surf. Sci.* **2022**, *602*, No. 154165.

(32) Wan, Q.; Guo, H.-Y.; Zhou, Y.-F.; Jiang, J.-N.; Chen, W.; Zheng, J.-F.; Shao, Y.; Wang, Y.-H.; Zhou, X.-S. The Regulation Effect of Coordination Number on the Conductance of Single-Molecule Junctions. *J. Mater. Chem. C* **2024**, *12*, 60–65.

(33) Herrer, I. L.; Ismael, A. K.; Milán, D. C.; Vezzoli, A.; Martín, S.; González-Orive, A.; Grace, I.; Lambert, C.; Serrano, J. L.; Nichols, R. J.; Cea, P. Unconventional Single-Molecule Conductance Behavior for a New Heterocyclic Anchoring Group: Pyrazolyl. *J. Phys. Chem. Lett.* **2018**, *9*, 5364–5372.

(34) Schulze, B.; Schubert, U. S. Beyond Click Chemistry-Supramolecular Interactions of 1,2,3-Triazoles. *Chem. Soc. Rev.* **2014**, *43*, 2522–2571.

(35) Nasri, S.; Bayat, M.; Kochia, K. Strategies for Synthesis of 1,2,4-Triazole-Containing Scaffolds Using 3-Amino-1,2,4-Triazole. *Mol. Divers.* **2022**, *26*, 717–739.

(36) Rauhut, G. Modulation of Reaction Barriers by Generating Reactive Intermediates: Double Proton Transfer Reactions. *Phys. Chem. Chem. Phys.* **2003**, *5*, 791–800.

(37) Joule, J. A.; Mills, K. *Heterocyclic Chemistry*, Fifth Edition; Wiley-Blackwell, 2010.

(38) Venkataraman, L.; Klare, J. E.; Tam, I. W.; Nuckolls, C.; Hybertsen, M. S.; Steigerwald, M. L. Single-Molecule Circuits with Well-Defined Molecular Conductance. *Nano Lett.* **2006**, *6*, 458–462.

(39) McNeely, J.; Miller, N.; Pan, X.; Lawson, B.; Kamenetska, M. Angstrom-Scale Ruler Using Single Molecule Conductance Signatures. *J. Phys. Chem. C* **2020**, *124*, 13427–13433.

(40) Pan, X.; Qian, C.; Chow, A.; Wang, L.; Kamenetska, M. Atomically Precise Binding Conformations of Adenine and Its Variants on Gold Using Single Molecule Conductance Signatures. *J. Chem. Phys.* **2022**, *157*, No. 234201.

(41) Pan, X.; Montes, E.; Rojas, W. Y.; Lawson, B.; Vázquez, H.; Kamenetska, M. Cooperative Self-Assembly of Dimer Junctions Driven by π Stacking Leads to Conductance Enhancement. *Nano Lett.* **2023**, *23*, 6937–6943.

(42) Nagahara, L. A.; Thundat, T.; Lindsay, S. M. Preparation and Characterization of STM Tips for Electrochemical Studies. *Rev. Sci. Instrum.* **1989**, *60*, 3128–3130.

(43) Fu, T.; Smith, S.; Camarasa-Gómez, M.; Yu, X.; Xue, J.; Nuckolls, C.; Evers, F.; Venkataraman, L.; Wei, S. Enhanced Coupling through π-Stacking in Imidazole-Based Molecular Junctions. *Chem. Sci.* **2019**, *10*, 9998–10002.

(44) Miao, Z.; Quainoo, T.; Czyszczon-Burton, T. M.; Rotthowe, N.; Parr, J. M.; Liu, Z.-F.; Inkpen, M. S. Charge Transport Across Dynamic Covalent Chemical Bridges. *Nano Lett.* **2022**, *22*, 8331–8338.

(45) Venkataraman, L.; Park, Y. S.; Whalley, A. C.; Nuckolls, C.; Hybertsen, M. S.; Steigerwald, M. L. Electronics and Chemistry: Varying Single-Molecule Junction Conductance Using Chemical Substituents. *Nano Lett.* **2007**, *7*, 502–506.

(46) Arnold, A.; Weigend, F.; Evers, F. Quantum Chemistry Calculations for Molecules Coupled to Reservoirs: Formalism, Implementation, and Application to Benzenedithiol. *J. Chem. Phys.* **2007**, *126*, No. 174101.

(47) Blum, V.; Gehrke, R.; Hanke, F.; Havu, P.; Havu, V.; Ren, X.; Reuter, K.; Scheffler, M. Ab Initio Molecular Simulations with Numeric Atom-Centered Orbitals. *Comput. Phys. Commun.* **2009**, *180*, 2175–2196.

(48) Wilhelm, J.; Walz, M.; Stendel, M.; Bagrets, A.; Evers, F. Ab Initio Simulations of Scanning-Tunneling-Microscope Images with Embedding Techniques and Application to C_{58}-Dimers on Au(111). *Phys. Chem. Chem. Phys.* **2013**, *15*, 6684–6690.

(49) Perdew, J. P.; Burke, K.; Ernzerhof, M. Generalized Gradient Approximation Made Simple. *Phys. Rev. Lett.* **1996**, *77*, 3865–3868.

(50) Lawson, B.; Zahl, P.; Hybertsen, M. S.; Kamenetska, M. Formation and Evolution of Metallocene Single-Molecule Circuits with Direct Gold- π Links. *J. Am. Chem. Soc.* **2022**, *144*, 6504–6515.

(51) Toher, C.; Filippetti, A.; Sanvito, S.; Burke, K. Self-Interaction Errors in Density-Functional Calculations of Electronic Transport. *Phys. Rev. Lett.* **2005**, *95*, No. 146402.

(52) Koentopp, M.; Burke, K.; Evers, F. Zero-Bias Molecular Electronics: Exchange-Correlation Corrections to Landauer's Formula. *Phys. Rev. B* **2006**, *73*, No.121403.

(53) Ke, S.-H.; Baranger, H. U.; Yang, W. Role of the Exchange-Correlation Potential in Ab Initio Electron Transport Calculations. *J. Chem. Phys.* **2007**, *126*, No. 201102.

(54) Quek, S. Y.; Venkataraman, L.; Choi, H. J.; Louie, S. G.; Hybertsen, M. S.; Neaton, J. B. Amine - Gold Linked Single-Molecule Circuits: Experiment and Theory. *Nano Lett.* **2007**, *7*, 3477–3482.

(55) Evers, F.; Korytár, R.; Tewari, S.; Van Ruitenbeek, J. M. Advances and Challenges in Single-Molecule Electron Transport. *Rev. Mod. Phys.* **2020**, *92*, No. 035001.

(56) Quek, S. Y.; Kamenetska, M.; Steigerwald, M. L.; Choi, H. J.; Louie, S. G.; Hybertsen, M. S.; Neaton, J. B.; Venkataraman, L. Mechanically Controlled Binary Conductance Switching of a Single-Molecule Junction. *Nat. Nanotechnol.* **2009**, *4*, 230–234.